



Testing the 'rare pit' hypothesis for xylem cavitation resistance in three species of *Acer*

Mairgareth A. Christman, John S. Sperry and Frederick R. Adler

Department of Biology, University of Utah, Salt Lake City, UT 84025, USA

Summary

Author for correspondence:

Mairgareth A. Christman

Tel: +1 801 585 0381

Email: m.christman@utah.edu

Received: 3 November 2008

Accepted: 28 December 2008

New Phytologist (2009) **182**: 664–674

doi: 10.1111/j.1469-8137.2009.02776.x

Key words: air seeding, cavitation, embolism, hydraulic architecture, inter-vessel pits, plant water transport, xylem.

- Eudicot angiosperms with greater vulnerability to xylem cavitation tend to have vessels with greater total area of inter-vessel pits, which inspired the 'rare pit' hypothesis: the more pits per vessel, by chance the leakier will be the vessel's single air-seeding pit and the lower the air-seeding threshold for cavitation to spread between vessels.
- Here, we demonstrate the feasibility of the hypothesis, using probability theory to model the axial propagation of air through air-injected stems. In the presence of rare, leaky pits, air-seeding pressures through short stems with few vessel ends in series should be low; pressures should increase in longer stems as more end-walls must be breached.
- Measurements on three *Acer* species conformed closely to model predictions, confirming the rare presence of leaky pits. The model indicated that pits air-seeding at or below the mean cavitation pressure (MCP) occurred at similarly low frequencies in all species. Average end-wall air-seeding pressures predicted by the model closely matched species' MCPs.
- Differences in species' vulnerability were primarily attributed to differences in frequency of the leakiest pits rather than pit number or area per vessel. Adjustments in membrane properties and extent of pitting per vessel apparently combine to influence cavitation resistance across species.

Introduction

Xylem sap is typically under pressures well below water vapor pressure. In this metastable state, it is vulnerable to 'cavitation' which is the abrupt transition to the stable vapor phase (Zimmermann, 1983). Cavitation within a xylem conduit usually leads to the withdrawal of liquid water from the conduit and diffusional equilibration of the expanding vapor void with the ambient air (Tyree & Sperry, 1989). An air-filled, or 'embolized', conduit no longer conducts water, and the process defines the range of xylem pressures that permit plant water uptake and all dependent processes, including net photosynthesis (Hubbard *et al.*, 2001). Cavitation pressures are relatively easy to measure, and often fall within the physiological range, and so the phenomenon can influence the physiology and ecology of plants (Tyree *et al.*, 1994; Maherali *et al.*, 2003). Because of this significance, there continues to be interest in discovering how cavitation occurs, and what anatomical or physiological features make it happen at different pressures in different species.

There is good evidence that cavitation caused by water stress results from air being sucked into the water-filled xylem

conduits by critically negative sap pressures (Zimmermann, 1983). Among the evidence for this 'air-seeding' mechanism is the observation that the blockage of water transport by gas filled conduits depends on the pressure *difference* between conduit sap pressure and surrounding air pressure, not the negative pressure of the sap itself (Cochard *et al.*, 1992; Salleo *et al.*, 1996; Sperry *et al.*, 1996). The same amount of blockage is observed whether the sap pressure is negative and air pressure is ambient, or the air pressure is raised and the sap pressure is ambient. Although many other mechanisms have been proposed for triggering cavitation (Pickard, 1981), none besides air seeding can explain this consistent experimental observation.

Where does the air enter? The xylem conduits, being dead, are skeletons with rigid, thick, lignified walls. Their typical porosity is probably too fine to explain observed air-seeding pressures (Oertli, 1971). Pits between conduits are logical candidates for air entry points: at pits, the only barrier is a thin pit membrane porous enough for water to flow across. Although these membranes (cellulosic meshes derived from the primary cell walls) also trap air-water interfaces, they are likely the first

part of the wall to leak air as sap pressures drop. Direct measurements of the air-permeability of pitted end-walls correspond well with observed cavitation pressures (Crombie *et al.*, 1985a,b; Sperry & Tyree, 1988, 1990; Jarbeau *et al.*, 1995). Accordingly, differences in pit structure should explain differences in cavitation resistance between conduits and species.

What aspect of pit structure dictates cavitation resistance? In gymnosperms, a torus seals off the pit aperture and the strength of the entire membrane apparently determines the strength of this seal (Sperry & Tyree, 1990). In angiosperms, where the pit seals entirely by capillary action, attention has naturally focused on membrane pore size. The capillary equation indicates that the largest pit membrane pore diameter (D) will dictate a pit's air-seeding pressure (P):

$$P = \frac{4T \cos \alpha}{D} \quad \text{Eqn 1}$$

where T is the surface tension of the sap and α is the contact angle between sap and pit membrane surface. But attempts to relate membrane porosity with observed air-seeding or cavitation pressures have come to different conclusions. In some cases, porosity corresponded well with air-seeding pressures (Jarbeau *et al.*, 1995), while in other cases, membrane pores were much smaller than the air-seeding diameter (Shane *et al.*, 2000; Choat *et al.*, 2003). A survey of 29 angiosperms showed only a weak correlation between vulnerability to cavitation and the hydraulic resistance of pit membranes, which should reflect their average porosity (Hacke *et al.*, 2006). Moreover, the correlation was the opposite of what might be expected: more vulnerable species had higher pit resistances (= less porous on average) than more resistant ones. The hydraulic resistances in this study indicated an average pore diameter in the 3–8 nm range (Wheeler *et al.*, 2005), much smaller than the *c.* 29–576 nm range required for pores air-seeding at measured cavitation pressures of between –10 and –0.5 MPa (Eqn 1, $\alpha = 0^\circ$).

The 'rare pit' hypothesis (also called the 'pit area' hypothesis) explains how average pit membrane porosity can be uncoupled from a much less porous air-seeding size range. The hypothesis states that pits with pores of air-seeding size are rare compared with the vast majority of pits with much narrower, air-tight pores (Hargrave *et al.*, 1994; Choat *et al.*, 2003; Wheeler *et al.*, 2005). Because of this, the vulnerability of a given conduit is heavily influenced by the number of pits it contains: the more pits that are present, by chance the leakier will be the leakiest pit per conduit. Because the single leakiest pit exposed to air determines the vulnerability of the conduit, the more pits that are present, the more vulnerable the conduit is to air-seeding. In the past we have termed this the 'pit area' hypothesis, but we choose the new 'rare pit' name because it emphasizes the probabilistic basis of the concept. Evidence for the hypothesis includes: the often observed rarity of pit membrane pores of air-seeding size; the lack of consistent correlation between indicators of mean membrane pore size and vulnerability to

cavitation; a significant correlation between inter-conduit pit area and vulnerability to cavitation; and a tendency (though often not statistically significant) for larger conduits to be more vulnerable to cavitation (Hargrave *et al.*, 1994; Choat *et al.*, 2003; Wheeler *et al.*, 2005; Hacke *et al.*, 2006).

In this paper we test the rare-pit hypothesis by measuring the actual air-seeding pressure across inter-vessel connections. In the following 'theory' section we use the mathematics of probability to demonstrate the feasibility of the hypothesis and show its dependence on rare, very leaky pits. We next apply the theory to the special case of air injection across stems of varying length, and present an anatomically specific model that predicts the air-seeding behavior across real stems. Finally, we test the model predictions within and across species. We used three species of *Acer* (*A. negundo*, *A. grandidentatum*, and *A. glabrum*) that differed substantially in their vulnerability to cavitation, but otherwise had qualitatively very similar xylem structure.

Description

Probability theory of the rare-pit hypothesis

The rare-pit hypothesis requires that in every species, regardless of cavitation resistance, there are a few 'leaky' pits with relatively low air-seeding pressures compared with the vast majority of very air-tight pits. The cumulative distribution function (cdf) of pit air-seeding pressure from all inter-vessel pits in the xylem of a species would therefore have a long tail (Fig. 1a). We refer to this as the 'pit cdf,' or symbolically as $F_m(p)$, where $F_m(p)$ is the probability that a pit has an air-seeding pressure \leq the air pressure, p . Different species could have somewhat different $F_m(p)$ distributions, but all would have a tail, and the important variation would be the thickness of this tail (Fig. 1a).

Although $F_m(p)$ distributions could differ between species, here we assume that, within a species, a single $F_m(p)$ applies equally to all vessels, meaning there is no strong bias towards leakier pits in some vessels or tighter pits in others. In this case, the cdf for the air-seeding pressure across a vessel wall is given by

$$F_c(p) = 1 - [1 - F_m(p)]^u \quad \text{Eqn 2}$$

where u is the number of inter-vessel pits per vessel. The bracketed $[1 - F_m(p)]^u$ term is the probability of a vessel with u pits having an air-seeding pressure greater than p , and thus 1 minus this term gives the probability of a vessel with an air-seeding pressure of p or less. As the number of pits per vessel increases, for example from 1 to 1000, by chance the leakier the vessel will become (Fig. 1b, solid lines and arrow, 'effect of increasing number of pits per vessel'; $F_c(p)$ calculated from the solid 'tail' $F_m(p)$ in Fig. 1a for $u = 1$ or 1000 pits).

The average air-seeding pressure of vessels in the xylem can be determined from the vessel wall cdf [$F_c(p)$] by converting

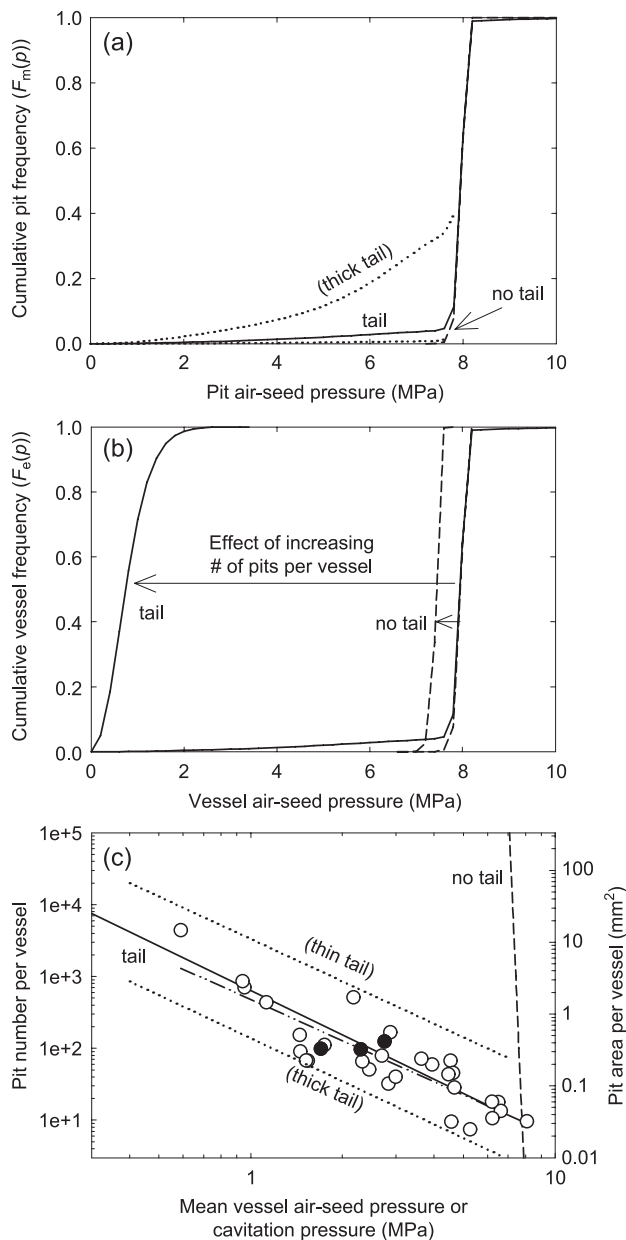


Fig. 1 Probability theory and the 'rare pit' hypothesis. (a) Cumulative distribution for inter-vessel pit air-seeding pressures [$F_m(p)$]. Solid and dotted lines represent curves with 'tails', indicating a low frequency of leaky pits as required by the rare-pit hypothesis; the dashed 'no tail' curve represents the case where all pits air-seed at a similarly high pressure (dashed). (b) Cumulative distributions for vessel air-seeding pressures ($F_e(p)$) calculated from pit distributions in (a) (Eqn 2). Distributions with (solid 'tail' curves) and without 'tails' (dashed 'no tail' curve) indicate different effects on vessel air-seeding pressure as the number of pits is increased from 1 to 1000 in the vessel. (c) Mean air-seeding pressure of vessels calculated from the range of $F_e(p)$ distributions in (b). There is a log-linear decline in vessel air-seeding pressure with increasing pit number (left axis) using the tailed pit distribution (solid 'tail' line). This matches the decline observed for cavitation pressure with increasing pit area per vessel in 29 eudicot species (open symbols, dashed-dotted line and right axis). Solid symbols are the three *Acer* species of the present study (left to right): *Acer negundo*, *A. glabrum*, and *A. grandidentatum*.

it to the corresponding probability density function and calculating the mean pressure of the distribution. The average air-seeding pressure of the vessels is a reasonable proxy for the mean cavitation pressure (MCP) of the xylem. We emphasize 'proxy' because it is not necessarily the case that a vessel will always air-seed when the xylem sap reaches the air-seeding pressure. In the intact stem, this will only occur if the vessel is adjacent to one that is already air-filled. The spatial linkage of vessels as well as the air-seeding pressure of their connections presumably must be taken into account to fully link pit properties to a xylem-level measure of cavitation resistance derived from vulnerability curves on whole stems (Loepfe *et al.*, 2007). Except for the special case of stem air-seeding pressures (see later discussion), we do not attempt to model this degree of complexity here.

The theory can be used to predict the sensitivity of average air-seeding pressure of vessels (and, by proxy, average cavitation resistance) to the number of pits per vessel. As the number of pits is increased, the average air-seeding pressure of vessels declines in a log-linear manner (Fig. 1c, solid 'tail' line). The slope of this log-linear relationship in our example is -2 and similar to the log-linear correlation observed between pit area per vessel and MCP for a large sample of eudicots (Fig. 1c, open symbols, data from Hacke *et al.*, 2006).

Although the data points in Fig. 1(c) show a strong trend towards greater vulnerability with more inter-vessel pitting there is considerable scatter. Variation in pit size could account for some of the scatter if pit number is more important than total pit area for influencing vulnerability. Another source of variation would be different $F_m(p)$ distributions between species. For example, some species could have a greater frequency of leaky pits (Fig. 1a, dotted 'thick tail' curve). Increasing or decreasing the thickness of the tail on the $F_m(p)$ cdf accommodates the scatter by shifting the intercept of the log-linear relationship while leaving the slope essentially unaltered (Fig. 1c, dotted 'thick tail' and 'thin tail' lines calculated from corresponding dotted $F_m(p)$ curves in Fig. 1a). These calculations suggest that variation in pit size and the rarity of leaky pits could explain variation in the link between pit area and vulnerability.

To complete the explanation of the pit area hypothesis, we consider the obvious alternative. All pits in all vessels could air-seed at a very similar pressure. In that case, the $F_m(p)$ cdf would be very steep with no tail (Fig. 1a, 'no tail' curve). Calculations show that the number of pits per vessel will have little influence on vessel cdf values ($F_e(p)$, Fig. 1(b), dashed curves and arrow, showing the effect of increasing pits/vessel from $u=1$ to 1000) and average vessel air-seeding pressures (Fig. 1c, dashed 'no tail' curve). In this scenario, variation between vessels or species in cavitation resistance would be associated with tightly coordinated alteration of membrane structure and porosity of all the pits.

Ideally, these two alternative explanations could be distinguished by measuring the air-seeding pressures of individual pits from many vessels and estimating the $F_m(p)$ distribution.

This would be technically quite challenging if not impossible. Instead, we measured the minimum air-seeding pressure of individual stems, injecting all vessels at one end with gas and noting the pressure at which the first bubbles streamed from a vessel at the other end after breaching the leakiest series of end-walls (see Methods). From these measurements, we determined the cdf for stem air-seeding pressure, which we refer to as the ‘stem cdf’ or $F_s(p)$. The probability theory developed below was used to predict how the $F_s(p)$ for stems of different lengths should depend on whether the $F_m(p)$ has a tail, as required by the rare-pit hypothesis, compared with the alternative of no tail.

Application of theory to the special case of stem air-seeding

Assume for simplicity that all vessels of a stem are of the same length and have the same number of inter-vessel pits. Further assume that they overlap extensively with each other in longitudinal files, such that all of the inter-vessel pitting is located on upstream and downstream ‘end-walls.’ The air-seeding pressure of a single axial file of vessels would tend to increase with stem length because by chance an ever-tighter end-wall would be encountered. If the air-seeding pressure of end-walls in a file are independent of one another, the cdf for file air-seeding pressure [$F_f(p)$] would be:

$$F_f(p) = F_c(p)^e \quad \text{Eqn 3}$$

where ‘ e ’ is the number of end-walls in series. Equation 3 indicates that the longer the stem and the greater the ‘ e ’, the more air-tight the stems will be. The $F_c(p)$ in Eqn 3 is given by Eqn 2 with u = the number of pits per end-wall, which is assumed to be half of the total pits per vessel. Because the $F_c(p)$ now refers specifically to the end-wall air-seeding pressure rather than that of the entire vessel, we hereafter refer to it as the ‘end-wall cdf’. The air-seeding pressure of an entire stem will also depend on the number of files in parallel. Adding more files in parallel should have the opposite effect as adding end-walls in series: stems should become leakier. For ‘ n ’ files in parallel, the cdf of stems air-seeding at pressure ‘ p ’ [$F_s(p)$] will be:

$$F_s(p) = 1 - [1 - F_f(p)]^n \quad \text{Eqn 4}$$

Eqn 4 predicts the expectation that more files (greater n) leads to greater $F_s(p)$ and leakier stems.

Equations 2–4 predict different $F_s(p)$ distributions depending on whether $F_m(p)$ has a tail or not. If a tail is present as required by the pit area hypothesis, the $F_s(p)$ changes dramatically with stem length (Fig. 2, ‘tail’, calculations based on the solid ‘tail’ $F_m(p)$ in Fig. 1a). In short stems with few end-walls for the air to cross axially, but many parallel files present, the average

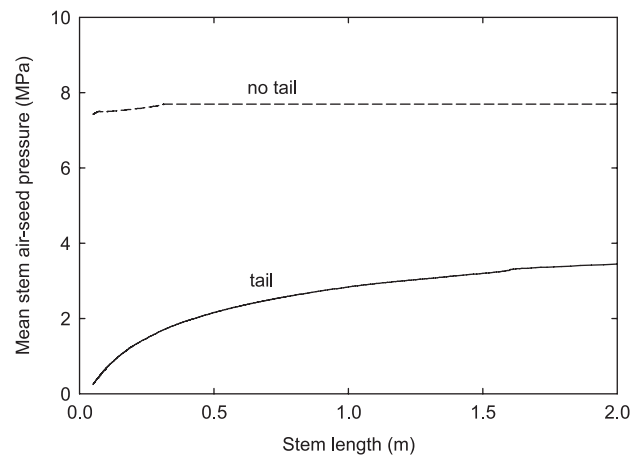


Fig. 2 Generalized prediction for how stem length should influence the minimum pressure required to inject air axially across the stem (stem air-seeding pressure). Predictions are calculated $F_s(p)$ values from Eqn 4 using 100 pits per end-wall, 100 files per stem, 1 cm vessel length, and were based on ‘tail’ and ‘no tail’ pit distributions of Fig. 1(a).

stem air-seeding pressure (calculated from the $F_s(p)$ distribution) is extremely low owing to the breaching of leaky pits. As stems are lengthened and more end-walls must be breached by the air, the chance of having multiple leaky end-walls in series goes down dramatically, and the average stem air-seeding pressure rises (Fig. 2). By contrast, with no tail present, stem air-seeding pressures are similarly high regardless of stem length because all pits have very similar air-seeding pressures (Fig. 2, ‘no tail’, based on corresponding $F_m(p)$ in Fig. 1a).

These alternative predictions do not depend on the simplifying assumption that all vessels of a stem are identical in length and in number of end-wall pits. In reality, there will be narrow and short vessels with relatively few pits, and wide, long vessels with lots of pits. To take this heterogeneity into account, we developed a probability model based on Eqns 2–4, and parameterized it for relevant anatomical traits.

Model description

Equations 2–4 can be modified to account for heterogeneous vessel length by discretizing vessels into length classes $i = 1$ to I . Eqn 2 becomes:

$$F_c(p, i) = 1 - [1 - F_m(p)]^{u_i} \quad \text{Eqn 5}$$

where u_i is the number of pits per end-wall for vessels of length class i . Eqn 3 becomes:

$$F_f(p, i) = F_c(p, i)^{e_i} \quad \text{Eqn 6}$$

Table 1 Model parameters and selected outputs

Species	Vessel length classes				Files per stem	P_{50} (MPa)	MCP (MPa)	EWP (MPa)	Weibull b	Weibull c
	Length class	Class mid-length (m)	Frequency	Pits per end-wall						
<i>Acer negundo</i>	1	0.00166	0.001329	566	1377 ± 263	1.70 ± 0.09	1.71 ± 0.11	1.88	5.26	8.61
	2	0.002729	0.007859	930						
	3	0.004485	0.026785	1528						
	4	0.007372	0.072153	2511						
	5	0.012116	0.158092	4127						
	6	0.019914	0.262241	6783						
	7	0.03273	0.28451	11 148						
	8	0.053793	0.156987	18 322						
	9	0.088412	0.030045	30 113						
<i>A. glabrum</i>	1	0.012028	0.016802	2811	664 ± 97	2.28 ± 0.14	2.27 ± 0.15	2.13	40.6	2.99
	2	0.014057	0.062402	3285						
	3	0.016427	0.124075	3839						
	4	0.019196	0.184755	4486						
	5	0.022433	0.218071	5242						
	6	0.026215	0.197271	6126						
	7	0.030636	0.128399	7159						
	8	0.035801	0.054861	8366						
	9	0.041838	0.013364	9777						
<i>A. grandidentatum</i>	1	0.009554	0.012769	3414	813 ± 90	3.19 ± 0.58	3.22 ± 0.50	2.85	92.9	2.63
	2	0.011742	0.05068	4196						
	3	0.014431	0.108064	5157						
	4	0.017736	0.173596	6338						
	5	0.021798	0.220351	7789						
	6	0.02679	0.2125	9573						
	7	0.032924	0.145228	11 765						
	8	0.040464	0.062426	14 460						
	9	0.049731	0.014385	17 771						

Vessel length distributions show midpoints of $l = 9$ length classes and net frequency of vessels in stem cross-section per class. Pits per end-wall for each class (u_i , Eqn 5) were estimated from the species' average pit area per vessel, average area per pit, and assuming that pit number was proportional to vessel length. Total files per stem is the average number of vessels at the injected point; multiplying this by the frequency of vessels in each length class gave the number of vessel files for each length class (n_i , Eqns 6, 7). Pressures at which 50% loss of conductivity occurred (P_{50}) and mean cavitation pressures (MCP) were not parameters or outputs of the model but are shown for comparison with the model output of mean air-seeding pressure of end-walls (EWP, from Eqn 5). The Weibull ' b ' and ' c ' parameters (Eqn 8) providing the best fit of Eqn 7 to stem air-seeding data are shown for each species.

where e_i is the number of end-walls in series for files composed of length class i . This assumes that vessels of a file have equal lengths. Eqn 4 then becomes

$$F_s(p) = 1 - \prod_{i=1}^I (1 - F_c(p, i))^{n_i} \quad \text{Eqn 7}$$

where n_i is the number of parallel files composed of vessels of length i . The measurement or estimation of vessel length classes $i = 1$ to I , $u(i)$, $e(i)$, and $n(i)$ is described in the Methods section. Resulting parameters are listed in Table 1.

We used the model to solve for the $F_m(p)$ that provided the best fit to data on $F_s(p)$. $F_s(p)$ data were measured on stems of varying lengths as describe in the Methods section, and the

mean stem air-seeding pressure at each stem length was used for comparison with the model prediction. We also compared the model's prediction of the average air-seeding pressure of vessel end-walls with the MCP measured from vulnerability curves. This told us how good a 'proxy' the end-wall air-seeding pressure is for the cavitation resistance of the xylem as a whole. The average air-seeding pressure of the end-walls was calculated by first determining the average for each length class (from its $F_c(p, i)$ distribution, Eqn 5) and then calculating the weighted average across length classes, weighting by the fraction of the total number of end-walls that were contributed by vessels in each length class.

To solve for the $F_m(p)$, we used a Weibull function to generate candidate distributions:

$$F_m(p) = 1 - e^{-(p/b)^c} \quad \text{Eqn 8}$$

where b is the pressure at $F_m(p) = 0.63$, and c determines the steepness of the distribution. To fit the model, b and c were varied until model error was minimized. The best-fit Weibull parameters (Table 1) concern the tail of the distribution; they do not necessarily represent the rest of the $F_m(p)$ distribution to which the model is insensitive. Model error was computed as the sum of the squares of the observed minus the modeled values, where the values were mean stem air-seeding pressures for each stem length. Error terms were weighted equally.

Methods

Plant material *Acer grandidentatum* Nutt. and *A. negundo* L. were collected from Red Butte Canyon, UT, USA (c. 40°47'N 111°48'W). *A. glabrum* Torr. was obtained from Millcreek Canyon, UT (c. 40°42'N 111°41'W). Stems were wrapped tightly in plastic and stored in a cold room in the laboratory until use (up to 1 wk).

Stem air-seeding pressure [$F_s(p)$] Stem air-seeding pressure is defined as the lowest gas pressure required to penetrate the closed end-walls of a stem. It was always measured by injecting air 'backwards' down the main stem (i.e. in the basipetal direction) from the base of the current year's extension growth. In this way, only the current growth ring was directly injected. This minimized effects of including older growth rings whose pit membranes may have become damaged by age or exposure to previous stress events (Sperry *et al.*, 1991; Hacke *et al.*, 2001; Stiller & Sperry, 2002). The seeding pressure was observed by placing the proximal end of the main stem under water and using a stereo microscope to detect the first bubble stream as pressure was raised. Nitrogen pressure was first applied at 30 kPa to detect any open vessels. Pressure was then increased in 100 kPa increments from a starting pressure of 100 kPa, waiting 1 min at each pressure. The first bubbles were typically seen within seconds of raising the pressure. Occasional observation indicated that if there were no bubbles after 1 min, waiting longer had no effect. Before air injection, stems were flushed for 30 min with 20 mM KCl at c. 70 kPa to remove any reversible embolism.

Stems of several lengths were tested from 'short' to 120 cm. 'Short' stems were systematically shortened to the point at which one open vessel was observed (air flowed through the stem at 30 kPa). The air-seeding pressure was recorded as the first stream of bubbles to appear as the pressure was raised from 100 kPa. Between 10 and 50 stems were measured at each length. In *A. negundo*, which typically had lower air-seeding pressures, we were able to obtain stem pressures for short, 20, 40, 80 and 120 cm lengths. In the other two species, we could not get complete data sets above 40 cm because pressures became too high (i.e. > 3.5 or 4 MPa) for the stems to be injected without

stems occasionally shooting out of the injection apparatus. At the longer lengths (> 40 cm) we also left side branches along the main stem intact because otherwise air could escape, reducing the pressure in the main axis where seeding was being measured.

Vessel length distributions and related model parameters

The silicone injection method was used to obtain vessel length distributions (Hacke *et al.*, 2007), from which vessel length classes were designated as required by Eqns 5–7. The silicone injection was done at the same position as the air-injection, basipetally down the main stem from the base of the current year's extension growth. Six stems per species were flushed with 20 mM KCl at c. 70 kPa to remove reversible embolism and injected under 50–75 kPa pressure overnight with a 10 : 1 silicone/hardener mix (RTV-141, Rhodia, Cranbury, NJ, USA). A fluorescent optical brightener (Ciba Uvitex OB, Ciba Specialty Chemicals, Tarrytown, NY, USA) was mixed with chloroform (1% w/w) and added to the silicone (1 drop g⁻¹) to enable detection of silicone-filled vessels in stem sections under fluorescent microscopy. After allowing the silicone to harden for several days, stems were sectioned at five places beginning 6 mm from the injection end and ending 8–12 cm back from the cut end. The fraction of silicone-filled vessels (N_L) at each length L was counted and the data were fitted with a Weibull function:

$$N_L = e^{-(kL)^c} \quad \text{Eqn 9}$$

where k and c are curve-fitting parameters. The best fit was then used to estimate the vessel length distribution. The equations given in Hacke *et al.* (2007), though producing the correct length distributions, were based on a misplaced parenthesis in Eqn 9 (only L was raised to the power ' c ') and so we report revised equations here. The second derivative of the Weibull multiplied by L gives the probability density of vessels of length L :

$$F_L = ck^c L^{(c-1)} e^{-(kL)^c} [c(kL)^c - c + 1] \quad \text{Eqn 10}$$

For the frequent case where ' c ' > 1, F_L becomes negative below a minimum length $L_{\min} = (1/k) [(c-1)/c]^{(1/c)}$. The L_{\min} represented the minimum vessel length. We also set a maximum vessel length $L_{\max} = L$ at $N_L = 0.0001$ and we adjusted F_L accordingly by dividing it by the integral of Eqn 10 from L_{\min} to L_{\max} . The Weibull cannot be integrated analytically, so numerical methods were used.

For each species, we used nine length classes, dividing them logarithmically to reflect the generally short-skewed distribution of vessel lengths (Zimmermann & Jeje, 1981). The upper limit of each length class (L_i) ' i ' was given as:

$$L_i = L_{\min} \left(\frac{L_{\max}}{L_{\min}} \right)^{(i/9)} \quad \text{Eqn 11}$$

Equation 10 was integrated between length class limits to obtain the fraction of vessels in each class [$F_L(i)$]. In all further calculations, L_i was set to the mid-length of the class instead of the upper limit (Table 1, 'Class mid-length'). Log-transformed mean lengths are reported, again because of the generally short-skewed length distributions.

Vessel lengths were used to determine the number of end-walls in series as required by Eqn 6 (e_i). We assumed that vessels making up a longitudinal file were of the same length class. The integer value of stem length divided by vessel length estimates the minimum number of end-walls in series for that vessel length class. For example, files of vessels 15 mm long would have a minimum of 13 end-walls in a stem 200 mm long (stem length/vessel length = 13.33). Assuming the end-walls are evenly distributed axially along the stem, a fraction (0.33) of the length class will have 14 end-walls. Thus, length classes were split to reflect the portions with the lower or higher end-wall number.

The model also required an estimate of the number of longitudinal files of vessels composing each length class (Eqn 7, n_i). The average total number of vessels (or files) in parallel at the air-injection point (base of current year's extension growth) was determined from cross sections (Table 1, 'files/stem'). Assuming that longitudinal files of vessels were composed of a single length class, their number was computed as the total number of files multiplied by the fraction of vessels in each length class computed by the integration of Eqn 10 (Table 1, 'frequency').

Inter-vessel pit parameters Average inter-vessel pit area and number per vessel was obtained by methods detailed in (Sperry *et al.*, 2007). Briefly, the fraction of inter-vessel walls occupied by pits was measured on longitudinal sections. The fraction of the vessel wall area in contact with adjacent vessels was estimated from cross-sections as the fraction of total vessel perimeter contacting adjacent vessels. The two fractions (pit area per inter-vessel wall, inter-vessel wall area per vessel wall area) multiplied gave the fraction of vessel wall area occupied by inter-vessel pits. This value in turn was multiplied by the average vessel wall area to give the average area of inter-vessel pits per vessel. The average vessel wall area was computed from the mean vessel length and mean diameter, assuming a cylindrical shape.

To assign the number of inter-vessel pits to each vessel length class (u_i , Eqn 5), we measured the average area per inter-vessel pit in each species. We then solved for the number of pits per vessel length required to match the average pit area per vessel for the species (Table 1, 'pits per end-wall').

Vulnerability curves The 'spin' method was used to obtain vulnerability curves for each species (Cochard, 2002; Cochard *et al.*, 2005; Li *et al.*, 2008). The 'spin' method allows for measuring conductivity while the stem is inside the centrifuge spinning at negative pressure and provides generally good agreement with the traditional 'gravity' method (Li *et al.*, 2008). The exact centrifugal apparatus and procedure is described in detail in Li *et al.* (2008). Six stems per species of *c.* 10 mm

diameter were trimmed under water to 27.5 cm length and bark was removed from each end. Stems were then flushed with 20 mM KCl at *c.* 70 kPa to remove reversible embolism. Initial maximum conductivity measurements were made with the standard 'gravity' method using 20 mM KCl and a pressure head of *c.* 4–6 kPa (Pockman *et al.*, 1995; Li *et al.*, 2008). Stems were then spun in a Sorvall RC-5C centrifuge (Thermo Fisher Scientific, Waltham, MA, USA) modified for the 'spin' method (Li *et al.*, 2008) at increasing speed until > 95% loss of conductivity was detected. The pressure at which there was 50% loss of conductivity (P_{50}) and the MCP were calculated from a Weibull function fit to the percentage loss of conductivity data for each stem and averaged for each species. MCP was calculated after first converting the Weibull function into a frequency distribution and calculating the mean of the distribution.

Results

Vulnerability to cavitation was greatest in *A. negundo* (MCP = 1.7 ± 0.1 MPa), followed by *A. glabrum* (MCP = 2.3 ± 0.1 MPa) and *A. grandidentatum* (MCP = 3.2 ± 0.5 MPa; means \pm SE). MCP and P_{50} were identical in each species (Table 1). In all three species, the conductivity actually increased when stems were in the centrifuge at their least negative pressures (relative to the initial reading measured by gravity head; Fig. 3). Therefore, P_{50} and MCP values were calculated relative to the maximum conductivity rather than the initial value.

Vulnerability to cavitation did not correspond with average pit area per vessel. The most cavitation-resistant species, *A. grandidentatum*, had the greatest pit area (0.42 mm^2), and the other two more vulnerable species had lower values, with *A. glabrum*

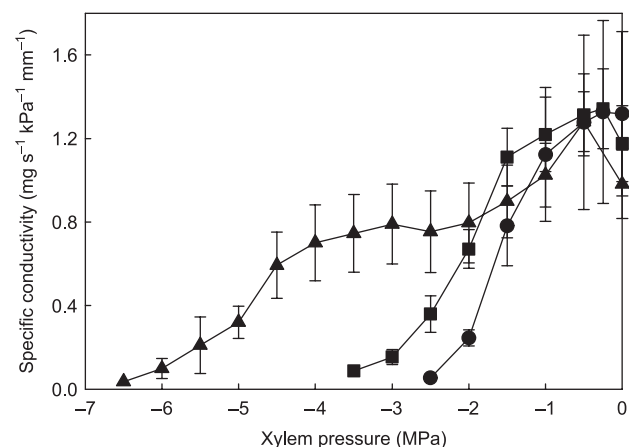


Fig. 3 Vulnerability curves of *Acer negundo* (circles), *A. glabrum* (squares), and *A. grandidentatum* (triangles). Curves show the drop in xylem conductivity measured during spinning in a centrifuge as cavitation was progressively induced. Conductivity at zero pressure (atmospheric) was measured by gravity feed. Conductivities are per stem cross-sectional area (means \pm SE, $n = 6$ stems). Pressure at 50% loss of conductivity and the mean cavitation pressure were calculated relative to the maximum conductivity measured, which for all species was not the initial gravity-feed value.

at 0.32 mm^2 and *A. negundo* at 0.33 mm^2 (Fig. 1c, solid symbols, right to left, respectively). However, the vulnerable *A. negundo* had the smallest pits ($17.2 \pm 0.90 \mu\text{m}^2$), and hence the greatest average number of pits per vessel (19 242). Nevertheless, decreasing pit numbers did not correlate with increasing cavitation resistance in the other two species. The most resistant one, *A. grandidentatum*, had an estimated 17 073 pits per vessel on average (area per pit = $24.2 \pm 1.10 \mu\text{m}^2$), whereas the more vulnerable *A. glabrum* had 10 832 estimated pits per vessel (area per pit = $29.8 \pm 0.99 \mu\text{m}^2$). The lack of a consistent relationship between either pit area or pit number with cavitation vulnerability theoretically requires differences in the $F_m(p)$ distributions between the species (e.g. thin vs thick tails; Fig. 1c).

Stem air-seeding pressures were consistent with the presence of rare, leaky pits as required by the rare-pit hypothesis. As

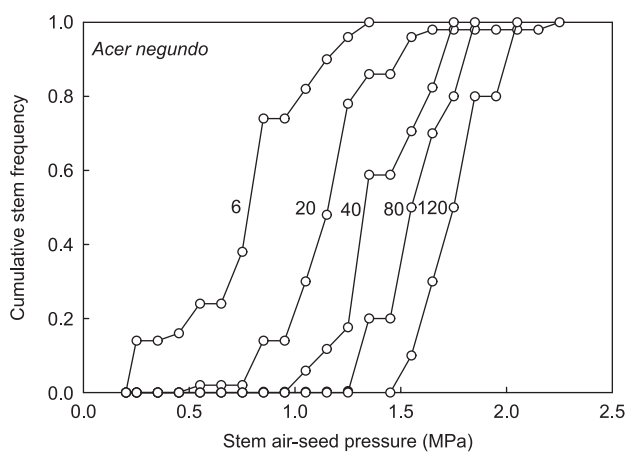


Fig. 4 Cumulative frequency of stems vs stem air-seeding pressure for *Acer negundo*. Stems of lengths ranging from 6 to 120 cm were injected at one end with nitrogen gas until the first bubble stream was detected at the other end.

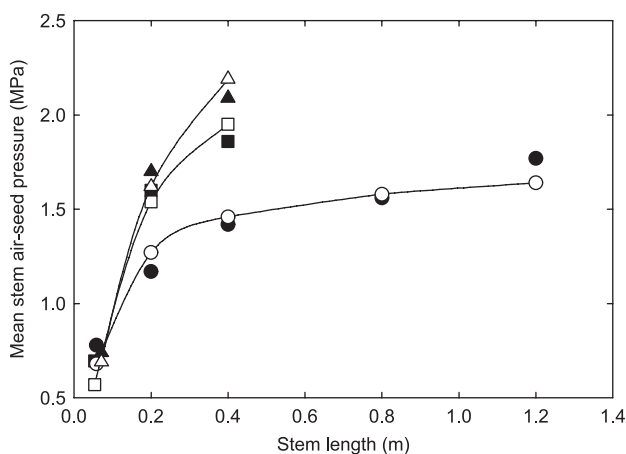


Fig. 5 Mean stem air-seed pressure vs stem length. Solid symbols are measured values (circles, *Acer negundo*; squares, *A. glabrum*; triangles, *A. grandidentatum*). Open symbols, curves, are the best-fits of the probability model from Eqn 7 using species-specific $F_m(p)$ distributions from a Weibull function (Eqn 8; Table 1).

predicted (Fig. 2), stem air-seed pressures increased strongly with increasing stem length in all three species (e.g. Fig. 4, data from *A. negundo*). The highest mean pressures were in the most cavitation-resistant species, *A. grandidentatum*. The lowest mean pressures were in the most vulnerable species, *A. negundo*; *A. glabrum* was intermediate (Fig. 5, solid symbols). Short stems with few end-walls had strikingly low mean air-seeding pressures that were statistically identical between all three species (Fig. 5, solid symbols; grand mean of $0.77 \pm 0.03 \text{ MPa}$; $F = 2.21$, $P = 0.11$).

In a few stems, we tested the repeatability of stem air-seeding pressure by immediately dropping the pressure after seeing the first bubble stream and then re-testing the same stem. We found no systematic change in stem air-seed pressure. This indicated the original air-seeding pressure was not caused by outright membrane rupture or else the subsequent pressures would have dropped. In two species (*A. negundo*, *A. grandidentatum*) we also tested short stems at different times of year. Regardless of whether they were tested in May (shortly after maturation), September, or January, the air-seeding pressure through the current year's growth of short stems averaged $< 0.85 \text{ MPa}$. Reported values were measured in January and February (Figs 4, 5).

The probability model was applied to the stem air-seeding data and cavitation pressures, using the parameters listed in Table 1 for each species. Mean vessel lengths (log-transformed) were identical in all three species at 2.2 cm, but *A. negundo* had a broader distribution, with vessels both shorter and longer than in the other two species (Table 1).

The model was successful in fitting the stem air-seeding data (Fig. 5, open vs solid symbols). Modeled vs measured stem air-seeding pressures gave a regression line not significantly different from 1 : 1, with $r^2 = 0.98$ (Fig. 6). The best model fit

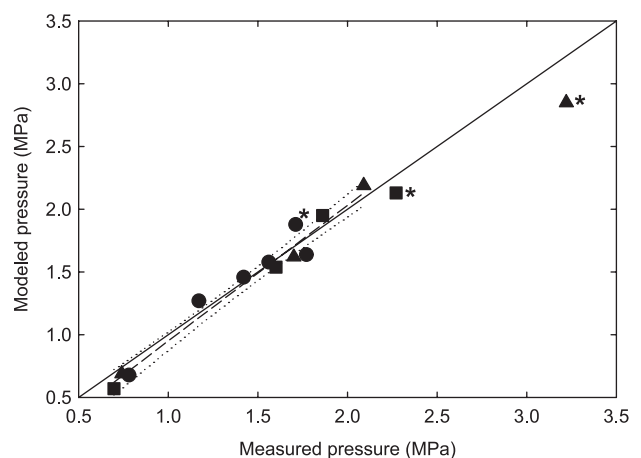


Fig. 6 Modeled vs measured stem air-seeding pressures (nonasterisked symbols, dashed regression line) did not differ from 1 : 1 (solid diagonal). The average air-seeding pressure of vessel end-walls (from Eqn 5) also closely matched measurements of MCP from vulnerability curves (asterisked symbols, not used in the regression). Circles, *Acer negundo*; squares, *A. glabrum*; triangles, *A. grandidentatum*.

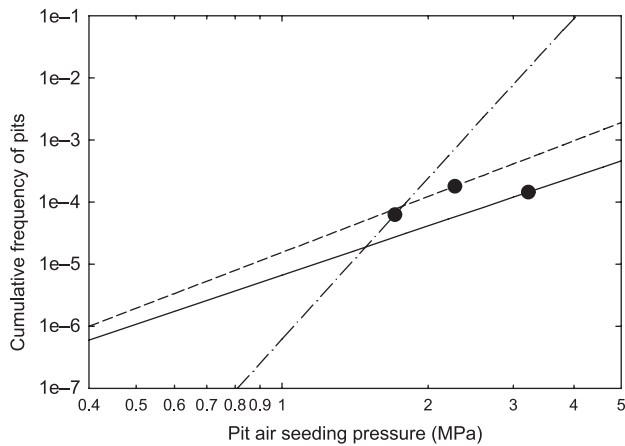


Fig. 7 Model pit distributions [$F_m(p)$, Eqn 8] providing the best fit to stem air-seeding pressures in each species. *Acer negundo* (dash-dotted line) had the thickest tail and was most vulnerable to cavitation, followed by *A. glabrum* (dashed line) and *A. grandidentatum* (solid line). Symbols show the similar frequency of pits air-seeding at or below the mean cavitation pressure (MCP) for each species.

was found for *A. glabrum*, followed closely by *A. grandidentatum* and *A. negundo*.

The average air-seeding pressure for vessel end-walls predicted by the model corresponded remarkably well with both the P_{50} and MCP of each species (Table 1; Fig. 6). The close correspondence indicated whole-stem cavitation pressure can be predicted from average air-seeding pressure of vessel end-walls, despite any complications of how air propagates from vessel to vessel in cavitating stems.

The Weibull-function $F_m(p)$ values (Eqn 8) that provided the best model fit indicated the presence of rare, leaky pits as predicted by the pit area hypothesis (Fig. 7; Table 1). The percentage of all pits that would air-seed at the MCP was extremely low and consistent between species: 0.006% in *A. negundo*, 0.014% in *A. grandidentatum*, and 0.018% in *A. glabrum* (Fig. 7, symbols; $F_m(p)$ shown on log scale to amplify the small-scale frequencies).

The model indicated that the pit cdf, or $F_m(p)$, was not identical across species, but shifted towards a thicker tail with greater vulnerability to cavitation. The most vulnerable species, *A. negundo*, was found to have the greatest proportion of leaky pits: a 'fatter' tail on its $F_m(p)$ distribution. Conversely, the most resistant species, *A. grandidentatum*, was found to have the rarest leaky pits, or the 'thinnest' tail (Fig. 7). In this group of three congeners, cavitation susceptibility was apparently more influenced by subtle differences in pit membrane porosity than by pit area or number.

Discussion

Our results strongly support the central requirement of the rare-pit hypothesis: that all species have a small percentage of exceptionally leaky pits. The most direct evidence for this was

that air-seeding pressure through short stems with few end-walls was not only statistically identical between the three *Acer* species (grand mean of 0.77 MPa), but also extremely low compared with the MCP (1.7–3.2 MPa). Clearly, all three *Acer* species have pits that are extraordinarily leaky. The observed increase in stem air-seeding pressure with increasing stem length (Fig. 5) indicates the rarity of these leaky pits: if they were present in every end-wall, stem length would have little effect on air-seeding pressure. As stems were lengthened, the variation in their air-seeding pressures also decreased substantially (Fig. 4, progressively narrower and steeper $F_s(p)$ cdf values left-to-right) as the effect of rare leaky pits was progressively masked by the majority of air-tight end-walls.

According to the model, single pits that air-seed at or below a species' MCP should be extremely rare; only 1 out of *c.* 10 000 pits would be this leaky based on the best-fit $F_m(p)$ distributions (Fig. 7). Searching for such a pit with the scanning electron microscope would be like looking for a needle in a haystack, which would explain why air-seeding pressures predicted from observed pore sizes tend to drastically exceed estimates based on measured P_{50} (Shane *et al.*, 2000; Choat *et al.*, 2003, 2008). The generally good fit of the model to measured stem air-seeding pressure (Fig. 6) provides more evidence that cavitation resistance is strongly influenced by the rare leaky pit rather than the comparatively air-tight properties of the vast majority of inter-vessel pits.

The results also emphasize that small variation in the frequency of rare pits can have a major effect on vulnerability to cavitation that is independent of the number or area of pits per vessel. This conclusion is evident from the scatter in the pit area vs vulnerability data (Fig. 1c, open symbols), and also from the lack of a relationship between pit area and vulnerability in our *Acer* species (Fig. 1c, solid symbols). Nor was there a consistent relationship when converting pit area to pit number. It is not known whether cavitation resistance is more sensitive to pit number or total pit area; replotting the pit area data in Fig. 1(c) in terms of pit number would begin to answer this question. Variation between species in membrane porosity potentially explains the residual scatter in the pit area or pit number relationship.

The average air-seeding pressure of end-walls predicted by the model corresponded remarkably well with the MCP measured from vulnerability curves, averaging within 10% of each other (Fig. 6, asterisked points). The end-wall air-seeding pressure indicates the potential for air-seeding given an adjacent air-filled vessel. Whether or not it actually air-seeds depends on how many air-filled vessels there are to begin with and their spatial distribution. The close correspondence we observed across species suggests that on average, the potential to air-seed is realized, meaning that air-seeding sites are not limiting. A detailed three-dimensional model of xylem conductivity and embolism propagation has recently been published (Loepfe *et al.*, 2007), and it would be useful to extend the model to test the effect of the rare-pit hypothesis on vulnerability curves.

The good fit of the model to the data suggests that any deviations from its many assumptions do not have major consequences. The assumption that vessels of a file have equal length is a reasonable simplification of the tendency for vessel diameter and length to be correlated. Less anatomically reasonable is the assumption that axial files of vessels are not linked by lateral pitting (Zimmermann, 1983). The generally good fit without accounting for lateral pits suggests that their main effect may have been shunting air from one axial file to the next, which functionally would still represent air propagating through a single file. There is no independent evidence for or against the assumption that the air-seeding pressure of pits in an end-wall are completely independent of other pits in the same end-wall, and that, similarly, the air-seeding pressure of end-walls in series are independent of one another (Eqns 5, 6). This touches on the important subject of how these leaky pits might arise in the first place.

The simplest possibility is that the leaky pits are 'mistakes,' an inevitable consequence of manufacturing tens of thousands of similar structures during vessel development. Deviations from the 'blueprint' could arise during the original deposition of the pit membrane in the living vessel, and also during the hydrolysis of protoplast during which the pit membrane can become modified (Dute & Rushing, 1990; Dute, 1994). Developmental mistakes may consist of extra-large pores or weak spots in the membrane which only become actual pores when the membrane is stressed (Choat *et al.*, 2004; Sperry & Hacke, 2004). Although our repeated measurements of air-seeding pressures indicated the membranes did not rupture during air-seeding, they do not tell us whether the pores were pre-existing or created by the initial air injection. It is unlikely that the leaky pits in our *Acer* material arose from the kind of severe cavitation-refilling cycles that cause 'cavitation fatigue' (Hacke *et al.*, 2001), because these leaky pits were present even in newly produced current year's secondary xylem.

If leaky pits result from inevitable developmental mistakes, a plant can 'control' its cavitation pressure by limiting the amount of pitting per vessel (the 'pit number strategy') and/or by limiting the rate or severity of mistakes during pit development (the 'pit porosity' strategy). Our results suggest that our three *Acer* species have adjusted their cavitation resistance primarily through differences in pit porosity rather than pit number or area per vessel. Anatomical observations indicate that reduced porosity may be achieved through greater membrane thickness, which in turn is correlated with greater wall thickness (Jansen *et al.*, 2009). Whether closely related species exploit the pit porosity strategy rather than the pit number strategy requires more studies of congeneric species. It does not appear to hold at the family level, because a survey of woody Rosaceae indicated that cavitation resistance was associated with differences in pit area rather than average membrane porosity (Wheeler *et al.*, 2005).

From the standpoint of minimizing flow resistance, both strategies for adjusting cavitation resistance can make sense.

In a wet habitat, where cavitation resistance is less important than in a dry habitat, increasing pitting per end-wall makes the vessels more vulnerable, but potentially reduces the end-wall resistance. Alternatively, keeping the pitting per end-wall constant and increasing the membrane porosity also makes more vulnerable xylem, but potentially reduces end-wall resistance (Sperry *et al.*, 2006). In this latter case, one must assume that the increase in frequency of leaky pits (which are probably too rare to influence end-wall flow resistance meaningfully) is coupled to a corresponding increase in the average membrane porosity which controls membrane flow resistance. If so, species adjust their entire $F_m(p)$ in concert, leaky and air-tight pits alike, rather than just changing the frequency of rare pits. A correlated adjustment in maximum and average membrane pore sizes was observed in a recent survey of pit membrane structure and function (Jansen *et al.*, 2009).

The results are clear that leaky pits are present, and they are relatively rare. But the crucial point that must be tested in future research is the role that these leaky pits actually play in determining a species' overall vulnerability to cavitation. Do these leaky pits truly occur independently in all vessels of the stem, and does their spatial distribution explain the propagation of gas through the system during natural cavitation or vulnerability curve experiments? Or are they confined to a few 'pathologically vulnerable' files of conduits and thus exert little influence on cavitation of the xylem as a whole? Is pit number per vessel more critical than pit area per vessel? Answering these questions with increasingly direct experimental approaches is a challenging goal.

Acknowledgements

We thank Duncan Smith, undergraduate of the University of Utah, for valuable assistance in measuring stem air-seeding pressures. Reid Persing provided valuable assistance with anatomical measurements. JSS acknowledges financial support from NSF-IBN-0743148.

References

- Choat B, Ball M, Luy J, Holtum J. 2003. Pit membrane porosity and water stress-induced cavitation in four co-existing dry rainforest tree species. *Plant Physiology* 131: 41–48.
- Choat B, Cobb AR, Jansen S. 2008. Structure and function of bordered pits: new discoveries and impacts on whole-plant hydraulic function. *New Phytologist* 177: 608–625.
- Choat B, Jansen S, Zwieniecki MA, Smets E, Holbrook NM. 2004. Changes in pit membrane porosity due to deflection and stretching: the role of vested pits. *Journal of Experimental Botany* 55: 1569–1575.
- Cochard H. 2002. A technique for measuring xylem hydraulic conductance under high negative pressures. *Plant, Cell & Environment* 25: 815–819.
- Cochard H, Cruiziat P, Tyree MT. 1992. Use of positive pressures to establish vulnerability curves: further support for the air-seeding hypothesis and implications for pressure-volume analysis. *Plant Physiology* 100: 205–209.

- Cochard H, Damour G, Bodet C, Tharwat I, Poirier M, Ameglio T. 2005. Evaluation of a new centrifuge technique for rapid generation of xylem vulnerability curves. *Physiologia Plantarum* 124: 410–418.
- Crombie DS, Hipkins MF, Milburn JA. 1985a. Gas penetration of pit membranes in the xylem of *rhododendron* and other species. *Planta* 163: 27–33.
- Crombie DS, Hipkins MF, Milburn JA. 1985b. Gas penetration of pit membranes in the xylem of *rhododendron* as the cause of acoustically detectable sap cavitation. *Australian Journal of Plant Physiology* 12: 445–454.
- Dute RR. 1994. Pit membrane structure and development in *Ginkgo biloba*. *IAWA Journal* 15: 75–90.
- Dute RR, Rushing AE. 1990. Torus structure and development in the woods of *Ulmus alata* michx., *Celtis laevigata* willd., and *Celtis occidentalis* l. *IAWA Bulletin* 11: 71–83.
- Hacke UG, Sperry JS, Feild TS, Sano Y, Sikkema EH, Pittermann J. 2007. Water transport in vesselless angiosperms: conducting efficiency and cavitation safety. *International Journal of Plant Sciences* 168: 1113–1126.
- Hacke UG, Sperry JS, Wheeler JK, Castro L. 2006. Scaling of angiosperm xylem structure with safety and efficiency. *Tree Physiology* 26: 689–701.
- Hacke UG, Stiller V, Sperry JS, Pittermann J, McCulloh KA. 2001. Cavitation fatigue: embolism and refilling cycles can weaken cavitation resistance of xylem. *Plant Physiology* 125: 779–786.
- Hargrave KR, Kolb KJ, Ewers FW, Davis SD. 1994. Conduit diameter and drought-induced embolism in *Salvia mellifera* greene (labiatae). *New Phytologist* 126: 695–705.
- Hubbard RM, Stiller V, Ryan MG, Sperry JS. 2001. Stomatal conductance and photosynthesis vary linearly with plant hydraulic conductance in ponderosa pine. *Plant, Cell & Environment* 24: 113–121.
- Jansen S, Choat B, Pletsers A. 2009. Morphological variation of intervessel pit membranes and implications to xylem function in angiosperms. *American Journal of Botany* 96: 409–419.
- Jarbeau JA, Ewers FW, Davis SD. 1995. The mechanism of water-stress-induced embolism in two species of chaparral shrubs. *Plant, Cell & Environment* 18: 189–196.
- Li YY, Sperry JS, Taneda H, Bush SE, Hacke UG. 2008. Evaluation of centrifugal methods for measuring xylem cavitation in conifers, diffuse- and ring-porous angiosperms. *New Phytologist* 177: 558–568.
- Loepfe L, Martinez-Vilalta J, Piñol J, Mencuccini M. 2007. The relevance of xylem network structure for plant hydraulic efficiency and safety. *Journal of Theoretical Biology* 247: 788–803.
- Maherali H, Pockman WT, Jackson RB. 2003. Adaptive variation in the vulnerability of woody plants to xylem cavitation. *Ecology* 85: 2184–2199.
- Oertli JJ. 1971. The stability of water under tension in the xylem. *Zeitschrift für Pflanzenphysiologie* 65: 195–209.
- Pickard WF. 1981. The ascent of sap in plants. *Progress in Biophysics and Molecular Biology* 37: 181–229.
- Pockman WT, Sperry JS, O'Leary JW. 1995. Sustained and significant negative water pressure in xylem. *Nature (London)* 378: 715–716.
- Salleo S, Lo Gullo MA, De Paoli D, Zippo M. 1996. Xylem recovery from cavitation-induced embolism in young plants of *laurus nobilis*: a possible mechanism. *New Phytologist* 132: 47–56.
- Shane MW, McCully ME, Canny MJ. 2000. Architecture of branch-root junctions in maize: structure of the connecting xylem and the porosity of pit membranes. *Annals of Botany* 85: 613–624.
- Sperry JS, Hacke UG. 2004. Analysis of circular bordered pit function i. Angiosperm vessels with homogenous pit membranes. *American Journal of Botany* 91: 369–385.
- Sperry JS, Hacke UG, Feild TS, Sano Y, Sikkema EH. 2007. Hydraulic consequences of vessel evolution in angiosperms. *International Journal of Plant Sciences* 168: 1127–1139.
- Sperry JS, Hacke UG, Pittermann J. 2006. Size and function in conifer tracheids and angiosperm vessels. *American Journal of Botany* 93: 1490–1500.
- Sperry JS, Perry AH, Sullivan JEM. 1991. Pit membrane degradation and air-embolism formation in ageing xylem vessels of populus tremuloides michx. *Journal of Experimental Botany* 42: 1399–1406.
- Sperry JS, Saliendra NZ, Pockman WT, Cochard H, Cruiziat P, Davis SD, Ewers FW, Tyree MT. 1996. New evidence for large negative xylem pressures and their measurement by the pressure chamber method. *Plant, Cell & Environment* 19: 427–436.
- Sperry JS, Tyree MT. 1988. Mechanism of water stress-induced xylem embolism. *Plant Physiology* 88: 581–587.
- Sperry JS, Tyree MT. 1990. Water-stress-induced xylem embolism in three species of conifers. *Plant, Cell & Environment* 13: 427–436.
- Stiller V, Sperry JS. 2002. Cavitation fatigue and its reversal in intact sunflower plants. *Journal of Experimental Botany* 53: 1155–1161.
- Tyree M, Davis S, Cochard H. 1994. Biophysical perspectives of xylem evolution – is there a tradeoff of hydraulic efficiency for vulnerability to dysfunction? *IAWA Journal* 15: 335–360.
- Tyree MT, Sperry JS. 1989. Vulnerability of xylem to cavitation and embolism. *Annual Review of Plant Physiology and Molecular Biology* 40: 19–38.
- Wheeler JK, Sperry JS, Hacke UG, Hoang N. 2005. Inter-vessel pitting and cavitation in woody rosaceae and other vesselless plants: a basis for a safety vs. Efficiency trade-off in xylem transport. *Plant, Cell & Environment* 28: 800–812.
- Zimmermann MH. 1983. *Xylem structure and the ascent of sap*. Berlin, Germany: Springer-Verlag.
- Zimmermann MH, Jeje AA. 1981. Vessel length distribution of some american woody plants. *Canadian Journal of Botany* 59: 1882–1892.